Kadam, Reshma ; Maas, Michael ; Rezwan, Kurosch

Selective, Agglomerate-Free Separation of Bacteria Using Biofunctionalized, Magnetic Janus Nanoparticles

Journal Article as: submitted version (Preprint)

DOI of this document*(secondary publication): https://doi.org/10.26092/elib/3200

Publication date of this document: 10/08/2024

* for better findability or for reliable citation

Recommended Citation (primary publication/Version of Record) incl. DOI:

Selective, Agglomerate-Free Separation of Bacteria Using Biofunctionalized, Magnetic Janus Nanoparticles. Reshma Kadam, Michael Maas, and Kurosch Rezwan. ACS Applied Bio Materials 2019 2 (8), 3520-3531
DOI: 10.1021/acsabm.9b00415

Selective, agglomerate-free separation of bacteria using biofunctionalized, magnetic Janus nanoparticles

Reshma Kadam[a], *Michael Maas*[a, b, *], *Kurosch Rezwan*[a,b]

*Corresponding author: email: michael.maas@uni-bremen.de, Tel. +49 421 218 – 64939, Fax. +49 - 421 218 – 64932

[a] Advanced Ceramics, University of Bremen, Am Biologischen Garten 2, 28359 Bremen, Germany

[b] MAPEX Centre of Materials and Processes, University of Bremen, 28359 Bremen, Germany

Keywords: Janus, nano, non-agglomerating, *E. coli*, separation

Abstract:

This study presents a scalable method for designing magnetic Janus nanoparticles which are capable of performing bacterial capture while preventing agglomeration between bacterial cells. To this end, we prepared silica-coated magnetite Janus nanoparticles functionalized with a bacteria-specific antibody on one side and polyethylene glycol chains on the other, using the established wax-in-water emulsion strategy. These magnetic Janus nanoparticles specifically interact with one type of bacteria from a mixture of bacteria via specific antigen-antibody interactions. Contrarily to bacterial capture with isotropically functionalized particles, the bacterial suspensions remain free from cell-nanoparticle-cell agglomerates owing to the passivation coating with polyethylene glycol chains attached to the half of the magnetic nanoparticles pointing away from the bacterial surface after capture. Selective magnetic capture of *Escherichia coli* cells was achieved from a mixture

with *Staphylococcus simulans* without compromising bacterial viability and with an efficiency over 80 %. This approach is a promising method for rapid and agglomeration-free separation of live bacteria for identification, enrichment and cell counting of bacteria from biological samples.

1. Introduction

With increasing resistance against antibiotics, bacterial contamination and infection are both long-standing and pressing issues in healthcare, nutritional industries and environmental engineering. Although new ways for eliminating pathogens have been developed in the last years, for example based on metal nanoparticles[1] or carbon nanomaterials,[2-4] the precise detection and efficient elimination of pathogenic bacteria remain significant challenges.[5-8] An especially promising approach for clinical diagnosis as well as environmental monitoring of pathogens is based on superparamagnetic iron oxide nanoparticles, which have become a staple in biomedicine in the last decades for cell labeling, separation and tracking.[9-12] Magnetic nanoparticles can be employed to capture and magnetically separate live bacteria from sewage water, biological fluids and similar systems for further analysis or elimination.[13-19] However, bare magnetic nanoparticles show low bacterial capture efficiency without further functionalization, especially due to their poor colloidal stability in biological media.[6] Consequently, the development of magnetic-nanoparticle-based systems with highly improved bacterial capture, separation and elimination efficiency is desired. To this end, various surface functionalizations of magnetic particles have been reported in recent publications, e.g. bacteria-specific antibodies,[6, 20-21] amino acids[11, 22], aminated silanes[23-25], drugs[24], surfactants[26] or synthetic ligands[27] which have improved capture efficiency to some extent.

Because the surfaces of bacteria are mostly negatively charged at physiological pH, efficient bacterial capture has been demonstrated with various positively charged nanoparticles that

efficiently bind to bacteria surfaces. In this respect, Fang et al. showed that the larger the number of amine groups on magnetic nanoparticles surfaces, the higher is the capture efficiency of the *Escherichia coli* (*E. coli*) cells.[28] Zhang et al. demonstrated the synthesis of polyallylamine functionalized cationic magnetic nanoparticles to isolate negatively charged bacteria and to identify which species actively took part in phenol degradation.[13] Bhaisare et al. used positively charged magnetic nanoparticles functionalized with an imidazole derivate to capture bacteria from blood.[29] As a more specific alternative to positively charged particles, several groups described the synthesis of antibody-functionalized magnetic polymer nanospheres for rapid capture and enrichment of one bacterial type.[6, 20-21]

However, since positively charged particles unspecifically bind to negatively charged bacterial surfaces, nanoparticle-bacteria complexes can result in agglomerated biomasses and rapid flocculation due to electrostatic heteroagglomeration. Similarly, particles that are isotropically functionalized with bacteria-specific antibodies cause agglomeration by forming bacteria-particle-bacteria bridges. Agglomeration and flocculation can strongly hamper isolation and analysis of bacterial species.[7, 23-25, 27-28, 30] Particularily, agglomeration can lead to incorrect bacterial cell counts.[7, 31-34] Furthermore, agglomerates of one bacteria type might potentially engulf other types of bacteria or other dispersed components of the bacteria suspensions.

Hence, for sensitive detection of bacteria along with realization of exact bacterial counts, we propose to use Janus particles, which are colloidal particles with two spatially separated properties on a single particle surface. Such Janus particles could be designed for bacteria-specific capture on one side and for preventing binding on the other side. In this respect, functionalization with polyethylene glycol (PEG) is a common strategy to suppress particle binding to cell surfaces and most biomolecules.[35-38]

Janus particles that are equipped with a combination of biofunctional properties on a single nanoparticle surface are gaining interest over the past several years.[25, 39-43] In the context of bacterial capture, Vilela et al. used magnesium Janus particles coated with magnetite and silver halves, which provide magnetic and bactericidal properties respectively. These so-called microbots are effective tools for rapid water disinfection.[44] Chang et al. reported the rapid detection of food-borne bacteria by using Janus nanorods consisting of a single magnetite nanoparticle attached to a mesoporous silica particle that was loaded with an antibacterial agent. While the reported anisotropic systems at this point seem to provide no clear functional benefit over magnetite particles fully embedded in a spherical structure or other isotropic designs, in these works, the authors clearly demonstrate the potential of sophisticated multifunctional nanostructures for such applications.[5, 8]

Here, we report the preparation of Janus particles for magnetic separation of one specific bacterial species from a mixture of bacteria with the added feature of avoiding agglomeration between bacteria. This feature is only possible because of the anisotropic nature of Janus particles. Specifically, we designed nano-sized SiO_2-coated magnetite (magnetite@SiO_2) Janus nanoparticles with bifunctional anisotropic properties. Antibodies against one particular bacterial species were immobilized on one side of the nanoparticles via biotin-streptavidin conjugation while the other side was functionalized with PEG chains via silanization, with the aim of passivating this side of the nanoparticle against agglomeration. To this end, we functionalized 45 nm SiO_2-coated magnetite nanoparticles with streptavidin-conjugated anti-*E. coli* antibody and with PEG-silane on opposing sides using the wax-in-water Pickering emulsion method.[40, 45] For the bacterial capture and separation experiments we used a mixture of *E. coli* and *Staphylococcus simulans (S. simulans).* The prepared Janus particles were characterized with DLS, TEM and suitable assays to quantify the surface functionalization. The bacterial capture system was analyzed via optical density

measurements for measuring capture efficiency, scanning electron microscopy (SEM) to understand the specificity of the nanoparticles and fluorescence microscopy to study agglomeration of the bacterial suspensions, along with assays for monitoring bacterial viability.

2. Experimental section

2.1 Chemicals

Oleic acid (product no. AAA16664AU) from Alfa-Aesar (Massacheusets, USA), 3 azidopropyltriethoxysilane (azidosilane , molecular weight 247.7 g/mol, product no. SIA0777.0) and 2-[methoxypolyethyleneoxy)propyl]trimetoxy-silane (PEG silane solution, 90%, 6-9 PE units, molecular weight 459-591 g/mol, product no. SIM6492.7) from Gelest *Inc*. (Frankfurt, Germany), dibenzylcyclooctyne-Cy3 (DBCO-Cy3 product no. 920) from Biomol GmbH (Hamburg, Germany), Fluoreporter Biotin Quantification Assay (product no. F30751) from Invitrogen (Karlsruhe, Germany), acetylene-PEG_4-Biotin (product no. CLK-TA105) from Jena Bioscience (Jena, Germany), Lynx Rapid Streptavidin Antibody Conjugation Kit (BioRad, LNK161STR) from BioRad (Oxford, United Kingdom), albumin from bovine serum fluorescein isothiocyanate conjugate (FITC BSA, product no. A23015) from ThermoFischer Scientfic (Massacheusets, USA), Anti-*E.coli* antibody (product no. ab137967) from Abcam (Cambridge, United Kingdom), gold-conjugated Streptavidin (O.D 10, product no. AC-10-04-15) from Cytodiagnostics (Ontario, Canada), paraffin wax (melting point 75°C to 90°C, product no. 8002-74-2) from Merck Millipore (Darmstadt, Germany), were purchased.

Aqueous ammonia (28% NH_3 in water, product number- 1336-21-6), tetraethyl orthosilicate (TEOS, product no. 78-10-4), 1-octadecene (product no. 112-88-9), iron (III) hexahydrate (product no. 10025-77-1), sodium hydroxide (product no. 1010-73-2), copper (III) sulfate pentahydrate (CuSO4, product no. 7758-99-8), hexadecyltrimethylammonium bromide (CTAB, product no.

855920), L-ascorbic acid (product no. A92902), Lysozyme from chicken egg white (product no. L6876), hexane (product no. 296090), cyclohexane (product no. 227048), ethanol (product no. 32205-M), 1-ocadecene (product no. O806), polyoxyethylene nonylphenylether (IGEPAL®CO-520, product no. 238643), phosphate buffered saline (PBS, product no. P4417) and 3-aminoproyl)triethoxysilane (APTES; product no. 440140), Tryptic soy broth (TSB, product no. 22092), Luria Bertani medium (LB, product no. L3022) were all purchased from Sigma Aldrich (Münich, Germany). All of the chemicals were used as-received and without any further purification. All investigations were made using double deionized water (ddH_2O, conductivity < 0.4 μS cm^{-1}) purified using SynergyUltra Water System (Millipore Corp., Massachusetts, USA).

2.2 Methods

2.2.1 Preparation of magnetite coated SiO_2 and surface functionalization

Magnetite nanoparticles were prepared using the thermal decomposition method.[46] Magnetite nanoparticles with a silica cover were prepared according to the protocol described by Ding et al.[47] In brief, the synthesis of magnetite@SiO_2 nanoparticles is based on a reverse micro emulsion using cyclohexane in the presence of IGEPAL®CO-520. The prepared nanoparticles are magnetically collected and washed several times with ethanol.

2.2.2 Preparation of nanoscale magnetite@SiO_2 Janus particles

For describing the step-wise functionalizations introduced on the Janus particles, we use the forward slash (/) to show the segregated sides on a single particle surface, and further functionalizations introduced on the respective sides are denoted by using a hyphen (-). For example, "PEG/azide-biotin-streptavidin-Ab magnetite@SiO_2" describes a silica-coated magnetite

particle that has been functionalized on one side with PEG and on the other side with azide, followed by biotin, followed by streptavidin, followed by biotin-conjugated antibody.

Surface functionalization of magnetite@SiO_2 with azide groups was performed using the method previously described by Lo Giudice et al. 9 ml of magnetite@SiO_2 (8.7 mg/mL) nanoparticle solution in ethanol was prepared using sonication. 0.5 mL of ethanol containing 21 µL of azidosilane were added dropwise to the nanoparticle solution at room temperature over a period of 60 min followed by heating for another 60 min at 90°C.[48] The azide-functionalized nanoparticles were then dried and used as required. Preparation of colloidosomes using azide-functionalized magnetite@SiO_2 was performed according to the method established by Granick et al.[45] and further adapted according to our previous work.[40] To impart the Janus feature, the 10 mg of the as-prepared particle-coated wax droplets were functionalized using 20 µl PEG silane following our established protocol.[40] Morphology of the solid wax droplets before and after functionalization was studied using the SEM. The concentration of the PEG-silane was twice the theoretically calculated monolayer coverage on the particle surfaces to ensure successful functionalization.

After dissolving the solid wax droplets using repeated chloroform and sonication steps, the azide/PEG magnetite@SiO_2 nanoparticles were extracted with water. Confirmation of the successful functionalization of PEG on the Janus nanoparticles was performed by adsorption of Lysozyme and FITC-BSA which was assessed by measuring the zeta-potential and residual protein concentrations, respectively.

Using the azide-acetylene copper mediated click chemistry reaction,[49] the linker acetylene-PEG_4-Biotin was attached to the azide-functionalized side of the Janus particles. This linker is required for the attachment of streptavidin-conjugated Anti-*E. coli* antibody. The PEG backbone in this case is used as a spacer to improve accessibility and flexibility of the conjugated antibodies. The linker

attachment was performed in ethanol following the protocol from reference.[40] After 16 h, the Janus nanoparticles were collected via magnetic separation and washed with ethanol.

To synthesize antibody-conjugated Janus nanoparticles, anti-*E. coli* antibody was first conjugated with streptavidin using the above-mentioned streptavidin-antibody conjugation kit. 10 μL of streptavidin anti-*E. coli* antibody (1 mg/ml) were incubated with 10 mg of azide-biotin/PEG magnetite@SiO_2 nanoparticles in PBS for 2 h at 4°C to allow for binding between the streptavidin conjugated antibody and the biotin groups on the Janus nanoparticles. Fully antibody functionalized nanoparticles (non-Janus) were used as the positive control in our experiments. Success of this functionalization step was assessed by conjugating the surface grafted biotin groups with gold-labeled streptavidin instead of the streptavidin-conjugated antibody for visualizing with TEM. The number of available biotin groups was quantified using the Fluoreporter biotin quantification kit. An overview of the multi-step synthesis is shown in Figure 1.

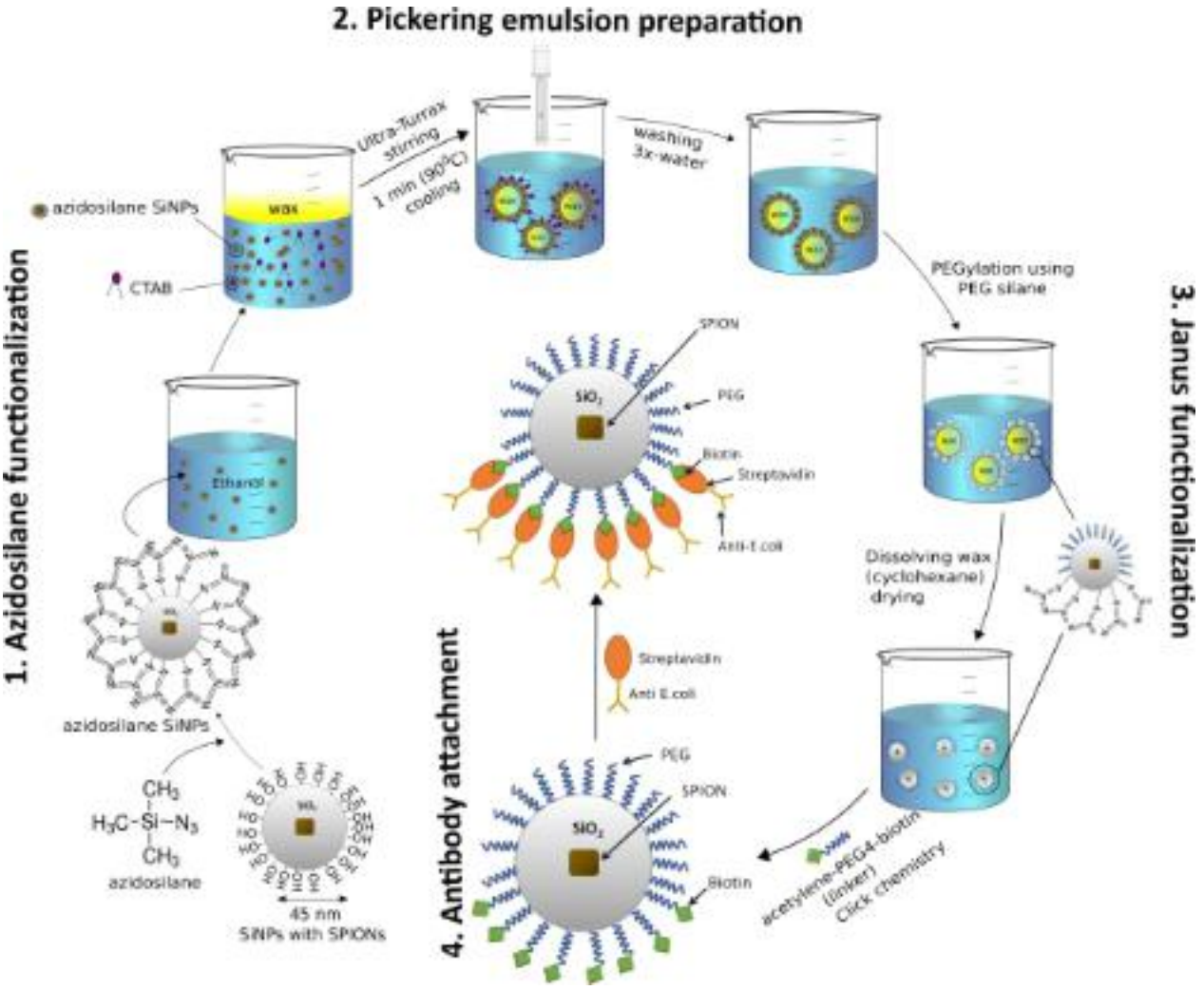

Figure 1. Schematic representation of the synthetic route of the preparation of magnetite@SiO_2 PEG/azide-biotin-streptavidin-Ab functionalized Janus nanoparticles. **Step 1**: azidosilane functionalization of magnetite@SiO_2 prepared using magnetite and TEOS. **Step 2**: Preparation of wax Pickering emulsion droplets using azide-functionalized magnetite@SiO_2 in the presence of CTAB. **Step 3**: PEGylation of the wax droplets was performed using PEG-silane to attach a second functionality on the exposed surfaces of the nanoparticle. The linker acetylene-PEG_4-biotin was attached using azide-acetylene click chemistry. **Step 4**: anti-*E. coli* antibody labeled with streptavidin was then used to produce magnetite@SiO_2 PEG/azide-biotin-streptavidin-Ab nanoparticles.

2.2.3 Characterization

The magnetism of the magnetite@SiO_2 nanoparticles was analyzed using Vibrating Sample Magnetometry (VSM, Microsense EZ9). The morphology of the Janus nanoparticles was examined using transmission electron microscopy (TEM, Supra 40, Zeiss, Germany). The nanoparticles were applied to copper grids (Plano GmbH, Germany). Particle size and zeta potential were measured using a Zeta Sizer Nano ZSP (Malvern instruments, USA) with dynamic and electrophoretic light scattering, respectively. The selective attachment of the Janus nanoparticles to the bacteria was studied using SEM (Supra 40, Zeiss, Germany) operated at 2.00kV. The optical density (OD) values of the magnetically separated pellet as well as the supernatant was measured at 595 nm to calculate capture efficiency of the Janus nanoparticles. Agglomeration effects of the Janus nanoparticles on *E. coli* and *S. simulans* after 1 h of separation was analyzed using fluorescence microscopy (Axiovert Imager M1, Zeiss, Germany).

2.3 Analysis of bacteria capturing

2.3.1 Selective recognition of *E. coli*

The pure cultures of *E. coli* K12 (DSMZ-1077) and *S. simulans* (DMSZ 20324) were purchased from "Deutsche Sammlung Mikroorganismen und Zell Kulturen" (Braunschweig, Germany) and were grown overnight in LB medium and TSB respectively at 37°C for 24 h at 150 rpm continuous shaking. Concentrations of *E. coli* and *S. simulans* individually and in combination were adjusted by measuring the optical density at 595 nm (OD_{595}) to obtain a total concentration of 10^7 cells/ml in phosphate buffered saline (PBS pH 6.2) according to McFarland standards.[7] The ability of the designed Janus particles to extract bacteria was tested by dispersing 100 µg of Janus nanoparticles in 1 ml *E. coli* suspension in the absence or presence of *S. simulans* in PBS buffer. The negative controls included the exposure of nanoparticles to *S. simulans* without *E. coli* to confirm the

specificity of the conjugated antibody. After 1 h of incubation, an external magnetic field was applied by placing a large neodymium magnet (50.8×50.8×25.4 mm, 10.5-12.0 kOe) under each bacteria-containing well to collect the Janus nanoparticles and the OD_{595} of the supernatant and the pellet was measured using a plate reader (Chameleon V, Hidex, Germany). Based on this data, the bacterial capture efficiency was calculated based on this equation:

$$\text{Capture efficiency}(\%) = \frac{\text{Initial [bacteria]O.D595 –magnetically seperated [bacteria]O.D595}}{\text{Initial [bacteria]O.D595}} \times 100$$

Bacterial suspensions without nanoparticles were analyzed as growth control.

To confirm the specificity of the nanoparticle adsorption on *E. coli*, the bacterial samples after exposure to the nanoparticles were used to prepare SEM samples.[5, 28, 50] The bacterial solution was deposited on a silicon wafer, which was previously functionalized with amino-propyl triethoxy silane (APTES)[51-52] to facilitate bacteria adsorption at the silicon substrate, followed by steps of glutaraldehyde fixation and ethanol dehydration.[3]

2.3.2 *In vitro* assessment of magnetic particle cytotoxicity:

Cell viabilities were tested based on adenosine triphosphate (ATP) quantification, colony forming units (CFU) counting and cell membrane integrity analysis. ATP quantification was performed using the luciferase-based BacTiterGlo™ assay (product no. G8231) purchased from Promega (Germany) which measures the ATP-activated bioluminescence of luciferin. Membrane integrity was assessed using the live/dead assay (Live/Dead, BacLight™, Life technologies, Germany). For the live/dead assay, a mixture of the dyes propidium iodide and SYTO©9 was added to the bacteria suspension after exposure to nanoparticles and then analyzed using fluorescence microscopy

(Axiovert Imager.M1, Zeiss, Germany). Colony forming units were counted based on the number of visible colonies on an agar plate. Adequate dilutions of bacterial suspensions are spread on an agar plate to obtain countable numbers of distinct colonies.

3 Results and Discussion

3.1 Preparation of azide-functionalized magnetite@SiO_2 nanoparticles

The multistep approach for the preparation of the Janus nanoparticles is illustrated in Figure 1. The initial magnetite nanoparticles were prepared using the thermal decomposition method. The mean hydrodynamic diameter (weighted by numbers) of the synthesized magnetite particles was 12 nm ± 2 nm, as obtained by dynamic light scattering (DLS) measurements (Figure S1). This diameter matches the range of diameters found via TEM. VSM analysis of magnetite nanoparticles showed superparamagnetic behavior with a saturation magnetization of 9 emu/g and an absence of magnetization hysteresis (Figure S1). The magnetite nanoparticles were then coated with a silica cover using TEOS by way of the reverse microemulsion and sol-gel method introduced by Ding et al.[47] The size of the magnetite@SiO_2 particles was 45.6 ± 2 nm which was again measured using DLS (Figure 2 **A** and **B** and Figure 3) and confirmed by TEM. The polydispersity index (PDI) of the DLS measurements was 0.15 ± 0.05, which points to a fairly narrow size distribution of the coated particles. VSM analysis of the coated particles showed that silica-coated particles are superparamagnetism with a moderate saturation magnetization of around 9 emu/g (Figure 2 **C**). The saturation magnetization of the uncoated iron oxide particles was in the same range (Figure S1).

The magnetite@SiO_2 particles were functionalized with azide groups using an azidosilane.[37] Azide functionalization caused an increase in the hydrodynamic size of the particles from 45.5 ± 2 nm to 50.4 nm ± 4.6 nm. A barely significant decrease in the negativity of the surface charge from

-32 ± 2.1 mV to -29.3 ± 2.4 mV was recorded (Figure 3), indicating that only a very small amount of active zwitterionic azide groups are present on the particle surface, which was comparable to our previous works and was confirmed using the azide quantification assay (Section 3.3).[40]

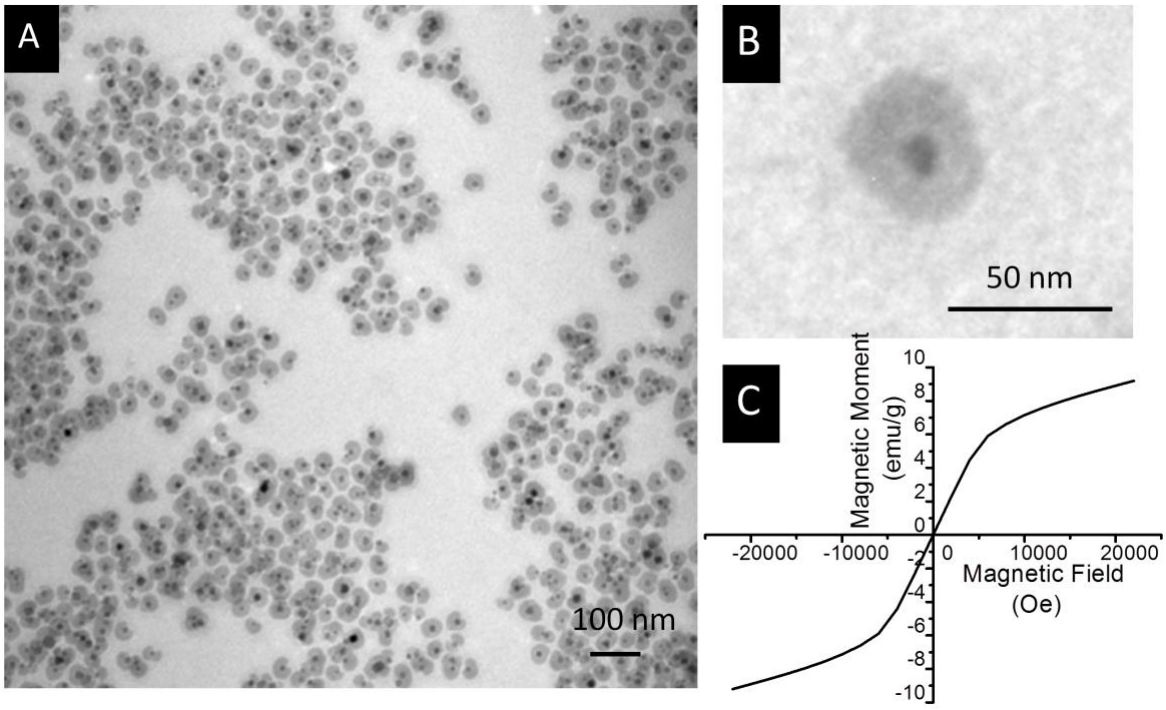

Figure 2. TEM micrograph of the prepared magnetite@SiO_2 particles. Magnetite nanoparticles were prepared using the thermal decomposition method and were further coated with silica using the reverse microemulsion method. (**A**)The as-prepared magnetite@SiO_2 particles had a hydrodynamic diameter of 45.6 ± 2 nm. (**B**) Close-up of the TEM micrograph of magnetite@SiO_2. (**C**) Magnetization of magnetite@SiO_2 showed typical superparamagnetic behavior.

Functionalization with azide was analyzed using the DBCO-Cy3 assay, which quantifies the fluorescent dye Cy3, which selectively binds to azide groups. The number of azide groups was further normalized to the particle surface area in nm^2, which is shown in Figure 3 **C**.[40, 53] DBCO-Cy3 attachment to the unfunctionalized magnetite@SiO_2 (0.18 ± 0.06 groups/particle) was negligible compared to the fully azide-functionalized nanoparticles (8.2 ± 0.4 groups/particle). The

rather low number of active azide groups/particle quantified in this work was comparable to our previous publication as well as to the work of LoGuidice et al.[40, 53]

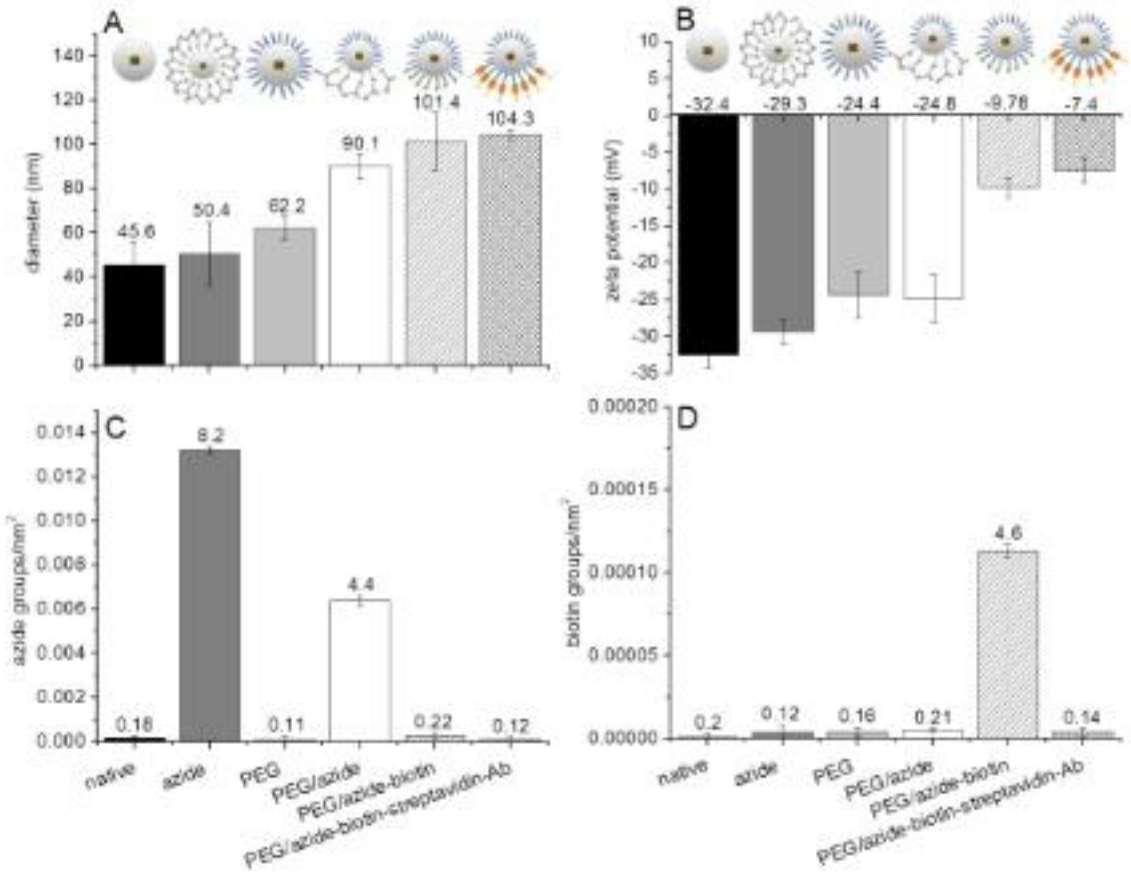

Figure 3. Size and surface properties of magnetite@SiO_2 in PBS before and after different functionalization. (**A**-**B**) Size and zeta potential overviews of the nanoparticles with different surface functionalization was measured via DLS. (**C-D**) Quantification of azide and biotin functional groups was done to confirm the success of the modification steps. The number of functional groups per particle is specified above each bar. Labels on (**C-D**) apply to (**A-B**) as well. The number of available azide and biotin groups on the particles was determined using the fluorescence of DBCO-Cy3 and the Fluoreporter® Biotin quantification kit, respectively. The label "native" represents unfunctionalized magnetite@SiO_2 nanoparticles.

3.2 Preparation of wax-in-water Pickering emulsions

Since particles at liquid-liquid[54-55] or air-water interface[56] tend to undergo free rotation, a solidifying oil phase, for example paraffin wax, is required for entrapping particles at emulsion droplet interfaces, which enables Janus functionalization of the exposed particle side.[45] In our case, the azide-functionalized nanoparticles were deposited on the surface of molten wax droplets, followed by cooling and solidifying the droplets, using the method established in our previous publication[40], which was adapted from the approach by Granick et al.[24] The azide-functionalized magnetite@SiO_2 particles (zeta potential -29.3 mV) were hydrophobized with the water-soluble surfactant CTAB to facilitate adsorption at the wax droplet surface. Compared to the original protocol, the surfactant concentration was roughly proportional to the increased surface area exhibited by the nanoscale particles.[40] In order to remove the excess of surfactant, which might interfere with the upcoming functionalization steps, the particle-bearing solidified wax droplets were washed several times with water until no more foaming of the washing water could be observed. These solid wax emulsions sustained the washing steps and the upcoming functionalization steps, which was also analyzed by SEM (Figure S2). SEM micrographs of particle-bearing wax particles show a size distribution of 500 nm to 50 μm (Figure 4 **A**). An irregular distribution of monolayers of nanoparticles was observed on the wax droplets (Figure 4 **A, inset**) and the azide-functionalized magnetite@SiO_2 remained partially embedded in the wax surface.[40] Gram quantities of wax Pickering emulsion droplets are produced using this method and hence can be used for large-scale preparation of Janus nanoparticles.

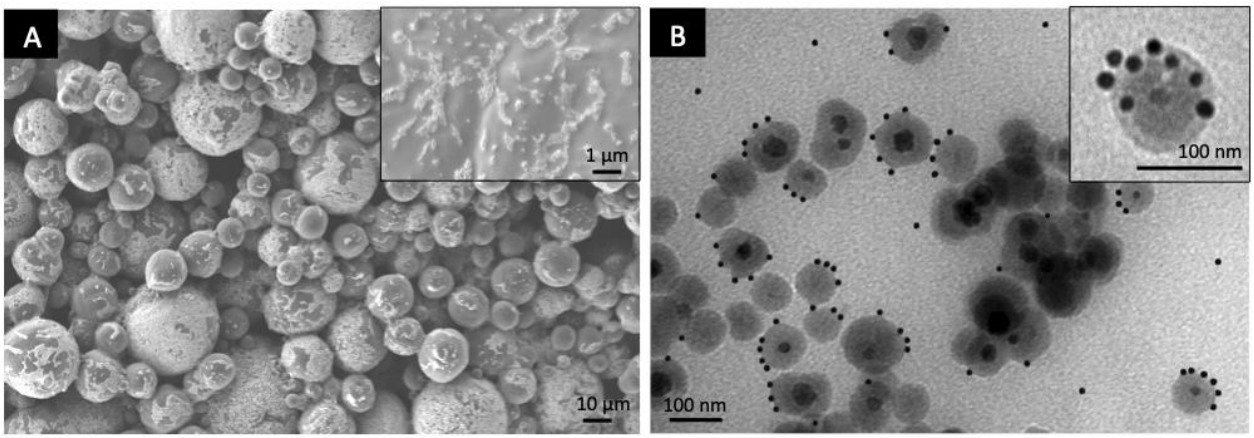

Figure 4. (**A**) SEM micrographs of wax Pickering emulsion droplets prepared using azide-functionalized magnetite@SiO_2 particles. Inset: close-up of the nanoparticles on the solid wax droplets. (**B**) TEM micrographs of the prepared Janus particles functionalized with PEG chains on one side and biotin groups on the other. Inset: close up of the as-prepared Janus nanoparticles. The presence of biotin on one side is confirmed using 10 nm gold-labeled streptavidin (see Figure S3 for additional images).

3.3 Janus functionalization with PEG-silane

To prepare bifunctional Janus particles, solid wax emulsions were dispersed in ethanol (10 mg/ml) and PEG-silane was added drop-wise to the solution under continuous stirring. After 2 h of incubation with the silane, minor loss of nanoparticles was observed from the wax particles (see Figure S2). A threefold excess of the silane concentration was used in order to ensure the attachment of the PEG groups in a dense surface coating. After functionalization with PEG groups, cyclohexane was used to dissolve the wax cores and release the PEG/azide magnetite@SiO_2 nanoparticles. DLS analysis of PEG/azide functionalized nanoparticles in PBS revealed a size of 90.1 ± 3 nm (PDI = 0.15) and a surface charge of -24.8 ± 2.3 mV.

After the preparation of the PEG/azide Janus nanoparticles, the amount of azide groups quantified was 4.6 ± 0.15 groups/particle, which is approximately half of the quantified groups on the fully azide-functionalized nanoparticles. This also confirms the Janus feature imparted using the partial masking by embedding in the surface of solid wax droplets.

PEG functionalization on nanoparticles has been widely studied to improve targeting efficiencies of nanoparticles by reducing protein corona formation.[57-58] Polymer chains arising from PEGylation on nanoparticles precludes them from interacting with other nanoparticles and components of biological systems, particularly surface-active proteins. This renders such nanoparticles less vulnerable to agglomeration and strongly reduces their interactions with cell surfaces. Therefore, PEG modification was analyzed by adsorption of the proteins fluorescein-isothiocyanate-modified bovine serum albumin (FITC-BSA) and lysozyme. 10 mg/ml nanoparticles of unfunctionalized, non-Janus (PEG functionalized) and Janus (azide/PEG) were incubated with 2 mg ml^{-1} FITC-BSA for 1 h. After incubation of the nanoparticles, the particles were washed twice and the amount of protein bound to the nanoparticles (Figure 5 **A**, black bars) and of the unbound protein (Figure 5 **A**, grey bars) were quantified photometrically. The amount of BSA adsorbed on 10 mg of anionic, unfunctionalized magnetite@SiO_2 particles was 900 ± 100 nmol g^{-1} of the respective nanoparticles. Adsorption of FITC-BSA (isoelectric point = 4.5,[59] slightly negatively charged at pH 6.2) was observed on negatively charged nanoparticles, which can be attributed to van-der Waals interactions, hydrophilic, hydrophobic, steric and structural interactions along with electrostatic interactions.[60-61] Lowest protein adsorption was recorded in case of non-Janus (full PEG) magnetite@SiO_2, as expected. In the case of the Az/PEG Janus nanoparticles, the amount of adsorbed FITC-BSA was 600 ± 50 nmol g^{-1}, which was reduced compared to that of the unfunctionalized (900 ± 100 nmol g^{-1}) but was higher than that of the non-Janus (200 ± 50 nmol g^{-1}) PEGylated nanoparticles. Summation of adsorbed and supernatant

concentrations of FITC-BSA roughly amounts to the initial concentration of FITC-BSA in all experiments (2000 nmol g^{-1}) considering potential losses of FITC-BSA during sample preparation. Additionally, we confirmed PEGylation by adsorbing the protein lysozyme (Figure 5 **B**). Lysozyme exhibits an isoelectric point of 11[62] and therefore is positively charged in PBS at pH 6.2. Consequently, it adsorbs on negatively charged magnetite@SiO_2 due to electrostatic interactions, which would be evidenced by the change in surface charge of the nanoparticles. The zeta potential of negatively charged unfunctionalized (-32 mV) and azide-functionalized (-29.3 mV) magnetite@SiO_2 changed to +10 ± 8 mV and to +8 ± 6.2 mV respectively. Hardly any alteration in the surface charge was observed in the case of non-Janus PEG functionalized nanoparticles, wherein the zeta potential values underwent a change from -24.4 ± 4.7 to -22.5 ± 2.6 mV. Lysozyme adsorption resulted in a moderate change in the zeta potential of the Janus nanoparticles (Az/PEG) from -24.8 ± 5 mV to -10 ± 2 mV.

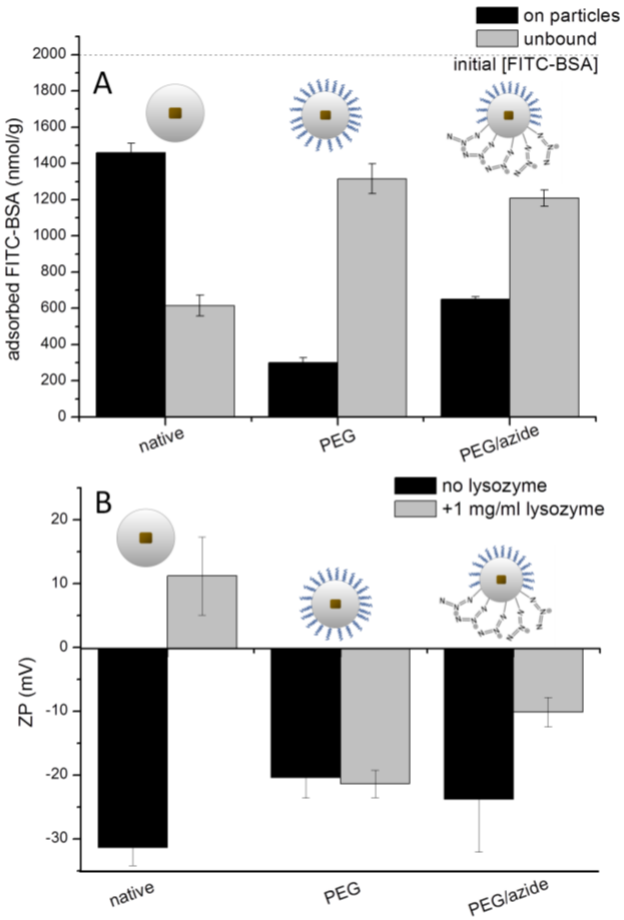

Figure 5. Characterization of PEG modification on magnetite@SiO_2 nanoparticles before and after functionalization with PEG. (**A)** Quantification of the amount of FITC-BSA adsorbed on the nanoparticles after PEGylation. (**B**) Zeta potential changes were analyzed before and after adsorption of lysozyme to qualitatively analyze the success of PEGylation on the respective nanoparticles mentioned under the respective bars.

3.4 Biotin functionalization

In order to attach the streptavidin-functionalized antibody for attaining selective *E. coli* capture, the PEG/azide functionalized Janus particles were coupled with the linker acetylene-$(PEG)_4$-biotin via copper mediated click chemistry. After this functionalization step, only a negligible amount of

DBCO-Cy3 attached to PEG/azide-biotin nanoparticles (0.22 groups/nm^2), indicating that no unreacted azide groups remain on the surface of the nanoparticles (Figure 3 **C**).

The number of biotin groups obtained via the Fluoreporter assay showed a negligible amount of biotin for all negative control measurements (native, full azide, full PEG and PEG/azide functionalized nanoparticles, Figure 3 **D**). An increase in the number of biotin groups was observed after the linker was attached to yield PEG/azide-biotin Janus nanoparticles 4.6 ± 0.16 groups/particle), which closely corresponds to the number of azide groups on the PEG/azide Janus particle surface, confirming the success of biotin functionalization. As an additional control, we synthesized fully biotin-functionalized magnetite@SiO_2 nanoparticles, which showed 8.2 ± 0.18 groups/particle (Figure S4 **D**).

Attachment of biotin groups on PEG/azide-biotin magnetite@SiO_2 caused a change in the surface charge of PEG/azide nanoparticles from -24.8 ± 3.2 mV to -9.78 ± 4.1 mV alongside an increase of size from 90.1 ± 4.3 nm to 101 ± 10 nm (Figure 3 **A**, **B**).[40]

To visually confirm the functionality of the biotin groups towards streptavidin conjugation on one hemisphere of the Janus particles, we incubated PEG/azide-biotin with gold-conjugated streptavidin.[39] As shown in Figure 4 **B** (overview) and 4 **C** (close-up), attachment of the streptavidin-gold on only one half of the nanoparticles was observed (see Figure S3 for additional images).

3.5 Antibody conjugation for PEG/azide-biotin-streptavidin-Ab Janus particles

The anti-*E. coli* antibody selected for this project specifically binds to the K antigen expressed by serotype *E. coli* K12.[63] After conjugating the anti-*E. coli* antibody with streptavidin following the protocol provided by the suppliers, PEG/azide-biotin functionalized nanoparticles are functionalized with the antibody on the azide-biotin hemisphere of the nanoparticle, leaving the

PEG chains on the other side of the particle. Size and zeta potential analysis of the PEG/azide-biotin-Ab-functionalized magnetite@SiO_2 yielded particles with a size of 104.3 ± 6.8 nm (Figure 3 **A**) and zeta potential of -7.4 ± 4.2 mV (Figure 3 **B**). The particles are colloidally stable despite the complex functionalities and multiple synthesis steps as evidenced by a fairly low PDI of 0.15. As an additional control, we also synthesized non-Janus anti-*E. coli* antibody-coated magnetite@SiO_2 nanoparticles with a size of 110.4 ± 5.7 nm (Figure S4 **A**) and a zeta potential of +7.45 ± 2.54 (Figure S4 **B**).

3.6 Aggregation of bacteria

The above described PEG/azide-biotin-streptavidin-Ab Janus particles were designed to capture one specific type of bacterium (*E. coli* K12 in this case) from a mixture of bacterial strains. To this end, the as-prepared particles were incubated with a 1:1 mixture of *E. coli* and *S. simulans* as well as with both strains individually. In order to visualize the bacteria with fluorescence microscopy, the cells were stained via the live/dead method. Green fluorescence shows viable bacterial cells with intact membranes (Figure 6). Dead cells (red fluorescence) were not observed in these experiments. The nanoparticles were exposed to *E. coli*, *S. simulans* or both for 1 h after which the live/dead staining procedure was carried out during the period of another 15 min. Figure 6 **A-C** show *E. coli*, *S. simulans* and the combination of both bacterial strains in the absence of nanoparticles. In the presence of the anionic unfunctionalized magnetite@SiO_2 nanoparticles, no bacterial agglomeration was observed in case of either the individual bacteria or a combination of both (Figure 6 **D**-**F**). After incubation of *E. coli* (Figure 6 **G**) and a mixture of *E. coli* and *S. simulans* (Figure 6 **I**) with nanoparticles fully functionalized with anti-*E. coli* antibody (non-Janus), clusters of bacteria were observed. *S. simulans* alone in the presence of anti-*E. coli* antibody-coated magnetite@SiO_2 remained unaffected from the clustering effect, which shows the specificity of the

antibody functionalized nanoparticles. The non-Janus antibody-functionalized particles most likely form cell-nanoparticle-cell bridges leading to the formation of bacterial flocs. As expected from our particle design, Janus functionalized PEG/azide-biotin-streptavidin-Ab magnetite@SiO_2 particles prevented agglomeration of *E. coli* cells in the presence (Figure 6 **L**) or absence of *S. simulans* (Figure 6 **J**). *S. simulans* alone remained unaffected by all types of nanoparticles (Figure 6 **B, E, H, K**).

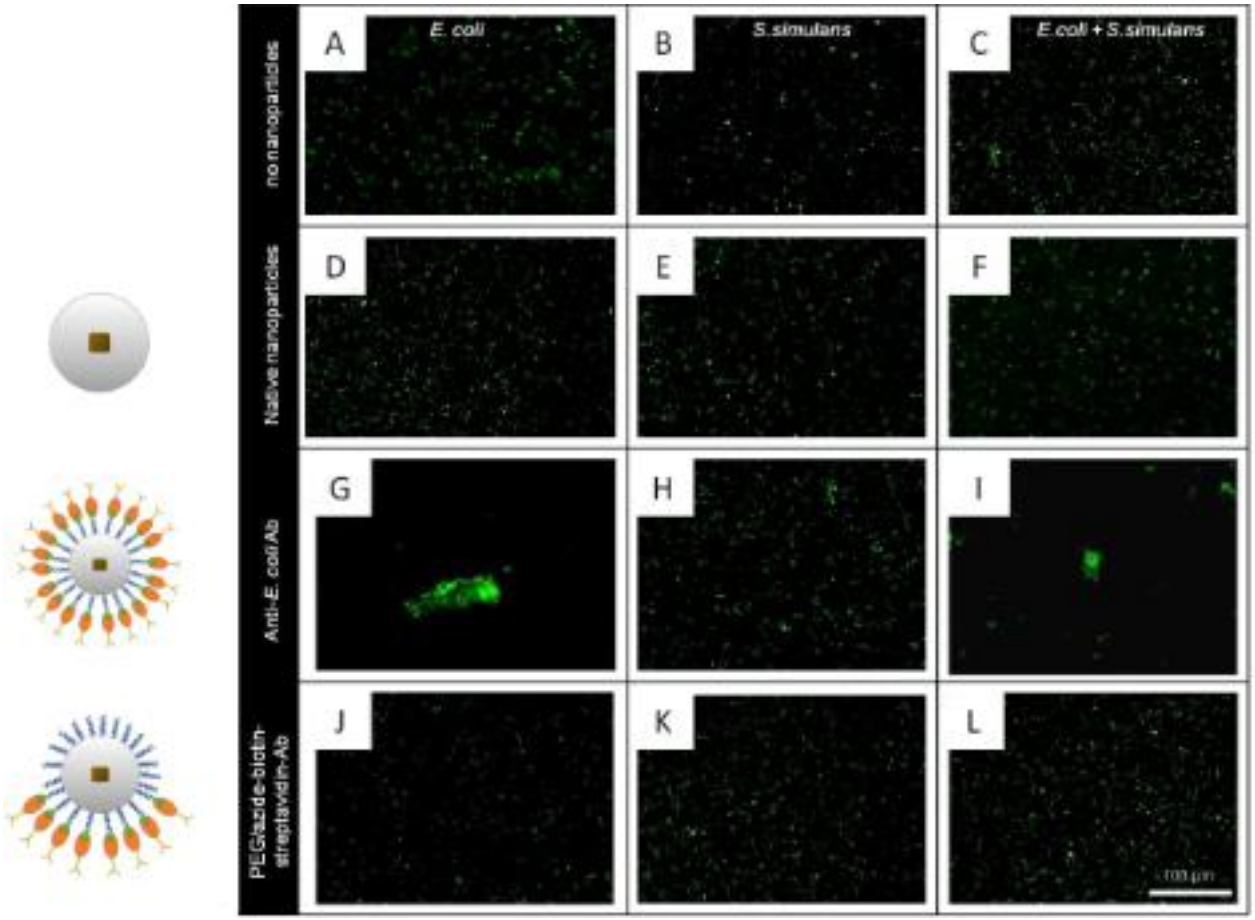

Figure 6. Fluorescence microscopy graphs of *E. coli* and *S. simulans* cells without (**A-C**) or with (**D-L**) the indicated nanoparticles for 1 h. Live/dead fluorescence staining was used to distinguish between viable (green) and dead (red) cells. The scale bar in **L** represents 100 µm and applies to all images. The label "native" represents magnetite@SiO_2 without any surface modification. Anti-

E. coli Ab nanoparticles indicate magnetite@SiO_2 nanoparticles that are fully functionalized with anti E. coli antibody (non-Janus), whereas PEG/azide-biotin-streptavidin-Ab nanoparticles indicate Janus nanoparticles with the respective functionalities each side.

3.7 Bacteria capture efficiency

By placing a neodymium magnet (50.8x50.8x25.4mm, 10.5-12.0 kOe) below the well plates with the bacteria/nanoparticle suspensions (Figure 7**A**), the magnetic particles could be extracted with varying amounts of bacteria captured by the particles (Figure 7**B**). After magnetic separation, residual and pellet concentrations of the bacteria were determined and capture efficiencies were calculated from this data (Figure 7**C**). In order to determine the amount of PEG/azide-biotin-streptavidin Ab-functionalized Janus nanoparticles required to magnetically separate *E. coli* cells (OD_{595}), we exposed 10^7 *E. coli* cells to increasing concentrations of particles (1-500 μg/ml) (Figure S5) over a period of 24 h. An increase in the capture efficiency was observed with increasing concentration of particles, until a maximum of capture efficiency of 82 ± 3 was recorded at 100 μg/ml which did not further increase with higher particle concentrations. At the same time, 100 μg/ml of PEG/azide-biotin-streptavidin-Ab functionalized Janus nanoparticles were incubated with 10^7 *E. coli* cells/ml at increasing time points ranging from 0-24h (Figure S6). Maximum bacterial capture efficiency of 85 ± 6 % was reached at 60 min. We measured the unspecific capture of 5 ± 3 % bacterial cells using negatively charged unfunctionalized magnetite@SiO_2. Capture efficiency from the *E. coli* suspension increased to 80 ± 5 % in the presence of PEG/azide-biotin-streptavidin-Ab functionalized particles. Similarly, the non-Janus nanoparticles showed capture efficiencies 82 ± 9 % from pure *E. coli*. Capture efficiency as recorded by similar publications with isotropic nanoparticles have values ranging from 90 - 100 %,[5, 11, 13, 25, 64-65] the slightly lower capture efficiency we measured is probably caused by the lower saturation magnetization of the magnetic

cores of the Janus nanoparticles. Additionally, adhesion of the antibody-functionalized particles might be reversible to some extent, leading to desorption of particles from the bacteria. In the presence of *S. simulans* alone, all particles showed unspecific capture efficiencies below 10 %. The Janus nanoparticles demonstrated a capture efficiency of 59 ± 6 % from mixtures of *E. coli* and *S. simulans*. Since only the optical density is measured, the test does not distinguish between the different types of bacteria. With this bacterial mixture, the efficiency of the fully anti-*E. coli* antibody-functionalized (non-Janus) nanoparticle was hardly different compared to that of the Janus nanoparticles with 58 ± 3 % (Figure 7**C**, light grey bars). Here, the overall capture efficiency is reduced because only 50% of the population of cells in the mixture is *E. coli* which binds to the antibody-functionalized particles with high selectivity, as established in the controls and in the agglomeration tests above.

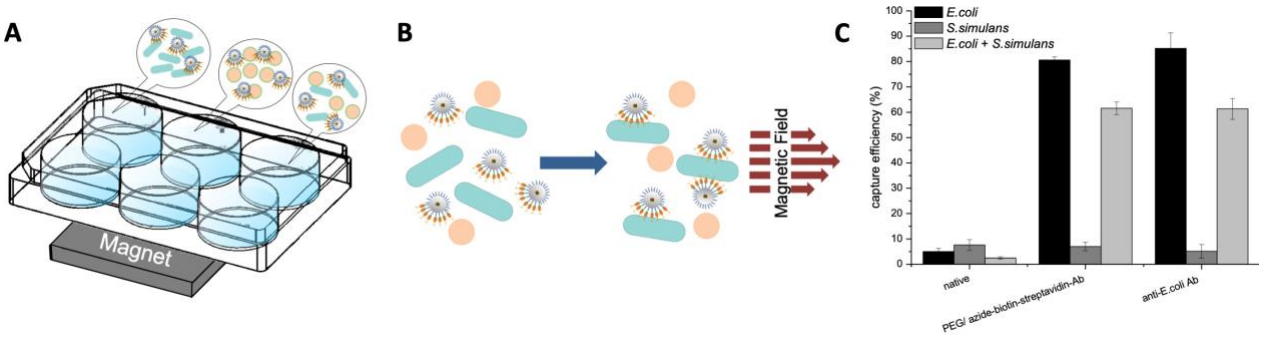

Figure 7. (**A**) Sketch of the experimental setup for the separation process using pure bacterial cultures as well as mixtures of bacteria. (**B**) Sketch of the capturing and separation principle of the prepared Janus nanoparticles. (**C**) Capture efficiency was measured using optical density measurements (OD_{595}). The label "native" represents magnetite@SiO_2 particles without any functionalization. Anti-*E. coli* Ab indicates particles that are fully functionalized with anti-*E. coli* antibody (non-Janus), whereas PEG/azide-biotin-streptavidin-Ab nanoparticles indicate the Janus nanoparticles.

Using SEM analysis we further confirmed the specificity of the Janus particles towards *E. coli* cells. A 1:1 mixture of *E. coli* and *S. simulans* was incubated without (Figure 8 **A-B**) and with Janus particles (Figure 8 **C-D**) in PBS buffer and the cells were later deposited on a previously functionalized positively charged silica substrate to facilitate bacteria attachment to the substrate surface. Bacteria specific adsorption of the Janus particles, as depicted in Figure 8 **D**, showed the affinity of the Janus particles towards *E .coli* cells only, as indicated by particles adhering in a rough layer at the surfaces of *E. coli* (Figure 8 **D**). *S. simulans* remained free from nanoparticles which is evident in the smooth surface of the bacteria in the SEM micrographs which remains unchanged after exposure to the particles.

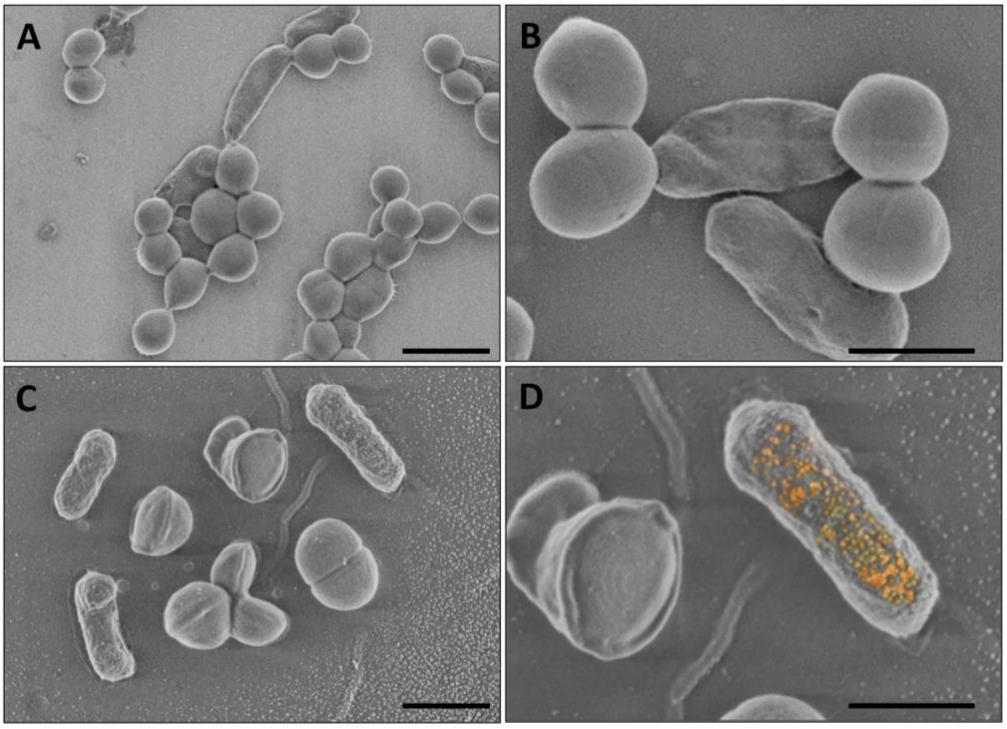

Figure 8. SEM micrographs of a mixture of *E. coli* and *S. simulans* incubated in the absence (**A,B**) or presence (**C,D**) of PEG/azide-biotin-streptavidin-Ab-functionalized magnetite@SiO_2 nanoparticles (Janus) to visualize selective attachment of nanoparticles on the bacteria. (**B**,**D**) Close-up view of the *E. coli* and *S. simulans*. (**D**) shows pseudo-colored (orange) nanoparticles selectively attached to the rod-shaped *E. coli*. The scale bars represent 1 µm.

3.8 Viability assessment

Viability analysis of *E. coli* and *S. simulans* after exposure to the unfunctionalized, Janus and non-Janus nanoparticles was performed using CFU counts and ATP quantification. To analyze the viability of the bacteria during the capturing procedure, CFU were separately determined from the supernatant and the pellet as obtained by magnetic separation as above. The pellet separated by the magnet was resuspended in fresh PBS and further spread on agar plates. CFU counts are made after 24 h of incubation at 37 °C, based on the principle that each viable cell forms a colony, which is then termed as a colony forming unit (CFU, Figure 9 **A**).

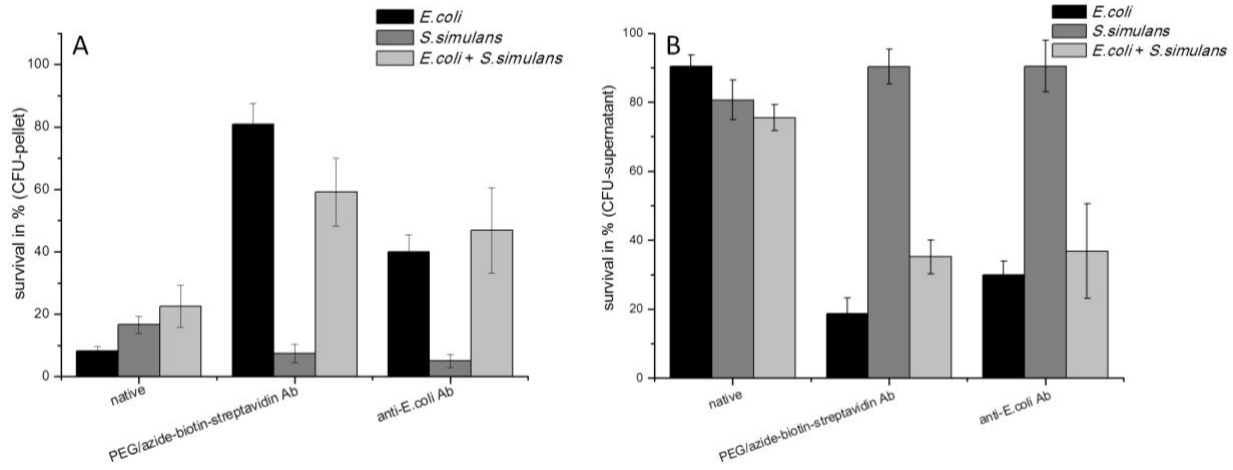

Figure 9. Viability of bacterial cells after exposure of 10^7 *E. coli* cells (OD_{595} 0.1) to 100 µg/ml of native, PEG/azide-biotin-streptavidin-Ab (Janus) and fully anti-*E. coli* Ab (non-Janus) functionalized nanoparticles in PBS buffer. After 1 h of magnetic capture, the cells captured as a pellet (**A**) and the remaining cells in the supernatant (**B**) were plated on agar plates to count the colony forming units (CFU). The data is expressed as % of the control (cells incubated without nanoparticles). All data are expressed as mean ± SD of values obtained from three independent experiments.

After the analysis of the respective supernatants after magnetic separation, we detected the remainder of the bacterial populations in the supernatant when normalized to the starting concentration of bacterial cells, therefore indicating that bacterial viability was not compromised after exposure to any of the tested nanoparticles (Figure 9 **B**). The capture efficiency quantified using CFU counts was generally comparable to the OD_{595} measurements (Figure 7 **C**), which indicates that all cells separated using such nanoparticles are viable. The clear exception were the non-Janus antibody-coated particles for which CFU counts from the *E. coli* suspension of only 40 ± 4% were observed which is significantly lower than the OD_{595} value for the bacterial capture of 85 ± 6 % shown in Figure 7. In the presence of the mixed suspension of *S. simulans* and *E. coli*, the non-Janus nanoparticles (fully anti-*E. coli*-Ab functionalized) show similarly decreased CFU counts of 42 ± 10 % compared to 58 ± 3 % in the OD analysis. However, this apparent reduction in viability was not observed in additional ATP tests with the luminescence assay BacTiterGlo (Figure 10 **A**). Here, exposure of *E. coli* to the non-Janus antibody-coated particles resulted in ATP levels of 82 ± 6 % and 12 ± 4 % at the pellet and supernatant, respectively. Similarly, exposure of *E . coli* and *S. simulans* to non-Janus antibody-coated particles yielded ATP levels of 60 ± 5 % and 40 ± 3% at the pellet and supernatant. Otherwise, results of the ATP-based metabolic activity assay were consistent with the CFU counts (Figure 9 **A** and **B**) as well as with the bacterial separation analysis via OD (Figure 7 **C**). Most likely, the decrease in bacterial cell counts in the CFU tests can be correlated to clustering of bacteria in the presence of the non-Janus antibody-coated particles, which was also qualitatively observed using fluorescence microscopy (Figure 6) and which leads to underestimation of cell counts with the CFU method.[7, 32, 34] CFU and ATP quantifications performed using other particles such as azide, PEG/azide and PEG/azide-biotin particles as controls showed that cell viability was not compromised in these cases (Figure S7).

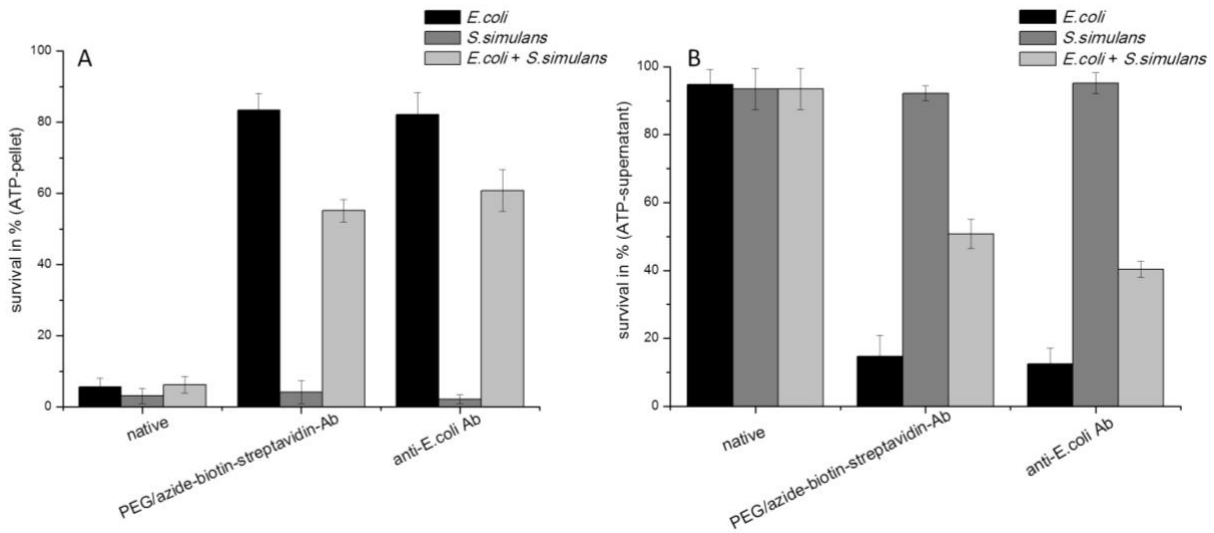

Figure 10. Viability of bacterial cells after exposure of 10^7 *E. coli* cells (OD_{595} 0.1) to 10 μg of unfunctionalized, PEG/Az-biotin-streptavidin-Ab (Janus) and fully anti-E.coli Ab (non-Janus) functionalized nanoparticles in PBS buffer. After 1 h of magnetic capture, the amount of ATP from the pellet (**A**) and the supernatant (**B**) was quantified using the luminescence assay BacTiterGlo. The data is expressed as % of the control (cells incubated without nanoparticles). All data are expressed as mean ± SD of values obtained from three independent experiments.

4. Conclusion

In summary, we presented the use of the wax-in-water Pickering emulsion method for the preparation of Janus particles for selective, agglomerate-free bacterial separation. The nanoscale magnetic Janus particles were half-coated with an antibody specifically against *E. coli* and accordingly showed over 80 % capture efficiency with this bacterium, which was comparable to that of nanoparticles fully functionalized with the antibody. Moreover, the prepared nanoparticles do not compromise the viability of the captured bacteria. By design, the Janus nanoparticles possess the capacity of carrying out bacterial capture without agglomeration between the bacteria, thereby significantly improving bacterial separation procedures for applications that require exact cell

551 counts and precise separation of bacterial species. Despite the seemingly complicated multi-step
552 process, the functionalization strategy is based on simple and established methods and can
553 potentially be easily scaled and adjusted. For example, by attaching other antibodies to the Janus
554 nanoparticles, this method can be tailored for the separation of any bacteria of interest from
555 biological samples of varying complexity.
556

557 **5. Acknowledgements**

558 The authors acknowledge the support of Petra Witte (University of Bremen, department of
559 Geosciences) with the SEM and Shruti Naik for help with the experimental work.
560

561 **6. Supporting Information**

562 Additional figures for particle characterization, capture efficiency measurements and viability data
563 have been included as a part of the supplementary information available from the ACS online
564 library or from the author.
565

7. Bibliography

1. Chernousova, S.; Epple, M., Silver as antibacterial agent: ion, nanoparticle, and metal. *Angew Chem Int Ed Engl* **2013,** *52* (6), 1636-53.

2. Kim, J.; Hyung-Mo, M.; Tung, S.; Hyun-Ho, L. In *Highly effective bacterial removal system using carbon nanotube clusters*, 2009 4th IEEE International Conference on Nano/Micro Engineered and Molecular Systems, 5-8 Jan. 2009; 2009; pp 1062-1064.

3. Wehling, J.; Dringen, R.; Zare, R. N.; Maas, M.; Rezwan, K., Bactericidal activity of partially oxidized nanodiamonds. *ACS Nano* **2014,** *8* (6), 6475-83.

4. Maas, M., Carbon Nanomaterials as Antibacterial Colloids. *Materials (Basel)* **2016,** *9* (8), 617.

5. Chang, Z. M.; Wang, Z.; Shao, D.; Yue, J.; Lu, M. M.; Li, L.; Ge, M. F.; Yang, D.; Li, M. Q.; Yan, H. Z.; Xu, Q. B.; Dong, W. F., Fluorescent-magnetic Janus nanorods for selective capture and rapid identification of foodborne bacteria. *Sensor Actuat B-Chem* **2018,** *260*, 1004-1011.

6. Chu, Y. W.; Engebretson, D. A.; Carey, J. R., Bioconjugated Magnetic Nanoparticles for the Detection of Bacteria. *Journal of Biomedical Nanotechnology* **2013,** *9* (12), 1951-1961.

7. Wehling, J.; Volkmann, E.; Grieb, T.; Rosenauer, A.; Maas, M.; Treccani, L.; Rezwan, K., A critical study: assessment of the effect of silica particles from 15 to 500 nm on bacterial viability. *Environ Pollut* **2013,** *176*, 292-9.

8. Chang, Z. M.; Wang, Z.; Lu, M. M.; Li, M. Q.; Li, L.; Zhang, Y.; Shao, D.; Dong, W. F., Magnetic Janus nanorods for efficient capture, separation and elimination of bacteria. *Rsc Advances* **2017,** *7* (6), 3550-3553.

9. Arruebo, M.; Fernández-Pacheco, R.; Ibarra, M. R.; Santamaría, J., Magnetic nanoparticles for drug delivery. *Nano Today* **2007,** *2* (3), 22-32.

10. Mahmoudi, M.; Sahraian, M. A.; Shokrgozar, M. A.; Laurent, S., Superparamagnetic iron oxide nanoparticles: promises for diagnosis and treatment of multiple sclerosis. *ACS Chem Neurosci* **2011,** *2* (3), 118-40.

11. Jin, Y. J.; Liu, F.; Shan, C.; Tong, M. P.; Hou, Y. L., Efficient bacterial capture with amino acid modified magnetic nanoparticles. *Water Research* **2014,** *50*, 124-134.

12. Teja, A. S.; Koh, P. Y., Synthesis, properties, and applications of magnetic iron oxide nanoparticles. *Prog Cryst Growth Ch* **2009,** *55* (1-2), 22-45.

13. Zhang, D. Y.; Berry, J. P.; Zhu, D.; Wang, Y.; Chen, Y.; Jiang, B.; Huang, S.; Langford, H.; Li, G. H.; Davison, P. A.; Xu, J.; Aries, E.; Huang, W. E., Magnetic nanoparticle-mediated isolation of functional bacteria in a complex microbial community. *Isme Journal* **2015,** *9* (3), 603-614.

14. Varshney, M.; Yang, L.; Su, X.-L.; Li, Y., Magnetic nanoparticle-antibody conjugates for the separation of Escherichia coli O157: H7 in ground beef. *Journal of food protection* **2005,** *68* (9), 1804-1811.

15. Huang, Y.-F.; Wang, Y.-F.; Yan, X.-P., Amine-functionalized magnetic nanoparticles for rapid capture and removal of bacterial pathogens. *Environmental science & technology* **2010,** *44* (20), 7908-7913.

16. Shan, Z.; Wu, Q.; Wang, X.; Zhou, Z.; Oakes, K. D.; Zhang, X.; Huang, Q.; Yang, W., Bacteria capture, lysate clearance, and plasmid DNA extraction using pH-sensitive multifunctional magnetic nanoparticles. *Analytical biochemistry* **2010,** *398* (1), 120-122.

17. Nakamura, N.; Burgess, J. G.; Yagiuda, K.; Kudo, S.; Sakaguchi, T.; Matsunaga, T., Detection and removal of Escherichia coli using fluorescein isothiocyanate conjugated monoclonal antibody immobilized on bacterial magnetic particles. *Analytical chemistry* **1993,** *65* (15), 2036-2039.

18. Widjojoatmodjo, M.; Fluit, A.; Torensma, R.; Keller, B.; Verhoef, J., Evaluation of the Magnetic Immuno PCR assay for rapid detection ofSalmonella. *European Journal of Clinical Microbiology and Infectious Diseases* **1991,** *10* (11), 935-938.

19. Matsunaga, T.; Nakayama, H.; Okochi, M.; Takeyama, H., Fluorescent detection of cyanobacterial DNA using bacterial magnetic particles on a MAG‐microarray. *Biotechnology and bioengineering* **2001,** *73* (5), 400-405.

20. Dinali, R.; Ebrahiminezhad, A.; Manley-Harris, M.; Ghasemi, Y.; Berenjian, A., Iron oxide nanoparticles in modern microbiology and biotechnology. *Critical Reviews in Microbiology* **2017,** *43* (4), 493-507.

21. Wen, C.-Y.; Jiang, Y.-Z.; Li, X.-Y.; Tang, M.; Wu, L.-L.; Hu, J.; Pang, D.-W.; Zeng, J.-B., Efficient Enrichment and Analyses of Bacteria at Ultralow Concentration with Quick-Response Magnetic Nanospheres. *ACS applied materials & interfaces* **2017,** *9* (11), 9416-9425.

22. Cheng, Y. X.; Liu, Y. J.; Huang, J. J.; Li, K.; Zhang, W.; Xian, Y. Z.; Jin, L. T., Combining biofunctional magnetic nanoparticles and ATP bioluminescence for rapid detection of Escherichia coli. *Talanta* **2009,** *77* (4), 1332-1336.

23. Gao, X. L.; Shao, M. F.; Xu, Y. S.; Luo, Y.; Zhang, K.; Ouyang, F.; Li, J., Non-selective Separation of Bacterial Cells with Magnetic Nanoparticles Facilitated by Varying Surface Charge. *Front Microbiol* **2016,** *7, 1891*.

24. Gu, H.; Xu, K.; Xu, C.; Xu, B., Biofunctional magnetic nanoparticles for protein separation and pathogen detection. *Chemical Communications* **2006,** (9), 941-949.

25. Wang, C.; Irudayaraj, J., Multifunctional Magnetic–Optical Nanoparticle Probes for Simultaneous Detection, Separation, and Thermal Ablation of Multiple Pathogens. *Small* **2010,** *6* (2), 283-289.

26. Chan, F. T.; Mackenzie, A. M., Advantage of using enrichment-culture techniques to isolate Campylobacter jejuni from stools. *The Journal of infectious diseases* **1984,** *149* (3), 481-2.

27. Lee, J.-J.; Jeong, K. J.; Hashimoto, M.; Kwon, A. H.; Rwei, A.; Shankarappa, S. A.; Tsui, J. H.; Kohane, D. S., Synthetic Ligand-Coated Magnetic Nanoparticles for Microfluidic Bacterial Separation from Blood. *Nano Letters* **2014,** *14* (1), 1-5.

28. Fang, W. J.; Han, C.; Zhang, H. B.; Wei, W. M.; Liu, R.; Shen, Y. X., Preparation of amino-functionalized magnetic nanoparticles for enhancement of bacterial capture efficiency. *Rsc Adv* **2016,** *6* (72), 67875-67882.

29. Bhaisare, M. L.; Abdelhamid, H. N.; Wu, B. S.; Wu, H. F., Rapid and direct MALDI-MS identification of pathogenic bacteria from blood using ionic liquid-modified magnetic nanoparticles (Fe3O4@SiO2). *J Mater Chem B* **2014,** *2* (29), 4671-4683.

30. Larsen, M. U.; Seward, M.; Tripathi, A.; Shapley, N. C., Biocompatible nanoparticles trigger rapid bacteria clustering. *Biotechnology progress* **2009,** *25* (4), 1094-1102.

31. Jiang, W.; Mashayekhi, H.; Xing, B., Bacterial toxicity comparison between nano-and micro-scaled oxide particles. *Environmental pollution* **2009,** *157* (5), 1619-1625.

32. Campanha, M. T.; Mamizuka, E. M.; Carmona-Ribeiro, A. M., Interactions between cationic liposomes and bacteria: the physical-chemistry of the bactericidal action. *J Lipid Res* **1999,** *40* (8), 1495-500.

33. Hansen, L. T.; Austin, J. W.; Gill, T. A., Antibacterial effect of protamine in combination with EDTA and refrigeration. *International journal of food microbiology* **2001,** *66* (3), 149-161.

34. Luo, P. G.; Tzeng, T.-R.; Qu, L.; Lin, Y.; Caldwell, E.; Latour, R. A.; Stutzenberger, F.; Sun, Y.-P., Quantitative analysis of bacterial aggregation mediated by bioactive nanoparticles. *J Biomed Nanotechnol* **2005,** *1* (3), 291-296.

35. Wilhelm, S.; Tavares, A. J.; Dai, Q.; Ohta, S.; Audet, J.; Dvorak, H. F.; Chan, W. C. W., Analysis of nanoparticle delivery to tumours. *Nature Reviews Materials* **2016,** *1*, 16014.

36. Torrice, M., Does Nanomedicine Have a Delivery Problem? *ACS Central Science* **2016,** *2* (7), 434-437.

37. Monopoli, M. P.; Aberg, C.; Salvati, A.; Dawson, K. A., Biomolecular coronas provide the biological identity of nanosized materials. *Nat Nanotechnol* **2012,** *7* (12), 779-86.

38. Shahabi, S.; Doscher, S.; Bollhorst, T.; Treccani, L.; Maas, M.; Dringen, R.; Rezwan, K., Enhancing Cellular Uptake and Doxorubicin Delivery of Mesoporous Silica Nanoparticles via Surface Functionalization: Effects of Serum. *ACS Appl Mater Interfaces* **2015,** *7* (48), 26880-91.

39. Yi, Y.; Sanchez, L.; Gao, Y.; Yu, Y., Janus particles for biological imaging and sensing. *Analyst* **2016,** *141* (12), 3526-39.

40. Kadam, R.; Zilli, M.; Maas, M.; Rezwan, K., Nanoscale Janus Particles with Dual Protein Functionalization. *Particle & Particle Systems Characterization* **2018,** *35* (3), 1700332.

41. Yanez-Sedeno, P.; Campuzano, S.; Pingarron, J. M., Janus particles for (bio)sensing. *Appl Mater Today* **2017,** *9*, 276-288.

42. Shao, D.; Li, J.; Zheng, X.; Pan, Y.; Wang, Z.; Zhang, M.; Chen, Q. X.; Dong, W. F.; Chen, L., Janus "nano-bullets" for magnetic targeting liver cancer chemotherapy. *Biomaterials* **2016,** *100*, 118-133.

43. Wang, Z.; Chang, Z.; Lu, M.; Shao, D.; Yue, J.; Yang, D.; Zheng, X.; Li, M.; He, K.; Zhang, M.; Chen, L.; Dong, W.-f., Shape-controlled magnetic mesoporous silica nanoparticles for magnetically-mediated suicide gene therapy of hepatocellular carcinoma. *Biomaterials* **2018,** *154*, 147-157.

44. Vilela, D.; Stanton, M. M.; Parmar, J.; Sánchez, S., Microbots decorated with silver nanoparticles kill bacteria in aqueous media. *ACS applied materials & interfaces* **2017,** *9* (27), 22093-22100.

45. Hong, L.; Jiang, S.; Granick, S., Simple method to produce Janus colloidal particles in large quantity. *Langmuir* **2006,** *22* (23), 9495-9.

46. Park, J.; An, K.; Hwang, Y.; Park, J. G.; Noh, H. J.; Kim, J. Y.; Park, J. H.; Hwang, N. M.; Hyeon, T., Ultra-large-scale syntheses of monodisperse nanocrystals. *Nat Mater* **2004,** *3* (12), 891-5.

47. Ding, H. L.; Zhang, Y. X.; Wang, S.; Xu, J. M.; Xu, S. C.; Li, G. H., Fe3O4@SiO2 Core/Shell Nanoparticles: The Silica Coating Regulations with a Single Core for Different Core Sizes and Shell Thicknesses. *Chemistry of Materials* **2012,** *24* (23), 4572-4580.

48. Giudice, M. C. L.; Meder, F.; Polo, E.; Thomas, S. S.; Alnahdi, K.; Lara, S.; Dawson, K. A., Constructing bifunctional nanoparticles for dual targeting: improved grafting and surface recognition assessment of multiple ligand nanoparticles. *Nanoscale* **2016,** *8* (38), 16969-16975.

49. Kolb, H. C.; Finn, M. G.; Sharpless, K. B., Click Chemistry: Diverse Chemical Function from a Few Good Reactions. *Angew Chem Int Ed Engl* **2001,** *40* (11), 2004-2021.

50. Joo, J.; Yim, C.; Kwon, D.; Lee, J.; Shin, H. H.; Cha, H. J.; Jeon, S., A facile and sensitive detection of pathogenic bacteria using magnetic nanoparticles and optical nanocrystal probes. *Analyst* **2012,** *137* (16), 3609-12.

51. Yadav, A. R.; Sriram, R.; Carter, J. A.; Miller, B. L., Comparative study of solution-phase and vapor-phase deposition of aminosilanes on silicon dioxide surfaces. *Mater Sci Eng C Mater Biol Appl* **2014,** *35*, 283-90.

52. Han, Y.; Mayer, D.; Offenhausser, A.; Ingebrandt, S., Surface activation of thin silicon oxides by wet cleaning and silanization. *Thin Solid Films* **2006,** *510* (1-2), 175-180.

53. Lo Giudice, M. C.; Meder, F.; Polo, E.; Thomas, S. S.; Alnahdi, K.; Lara, S.; Dawson, K. A., Constructing bifunctional nanoparticles for dual targeting: improved grafting and surface recognition assessment of multiple ligand nanoparticles. *Nanoscale* **2016,** *8* (38), 16969-16975.

54. Glaser, N.; Adams, D. J.; Böker, A.; Krausch, G., Janus Particles at Liquid−Liquid Interfaces. *Langmuir* **2006,** *22* (12), 5227-5229.

55. Fujimoto, K.; Nakahama, K.; Shidara, M.; Kawaguchi, H., Preparation of Unsymmetrical Microspheres at the Interfaces. *Langmuir* **1999,** *15* (13), 4630-4635.

56. McGorty, R.; Fung, J.; Kaz, D.; Manoharan, V. N., Colloidal self-assembly at an interface. *Materials Today* **2010,** *13* (6), 34-42.

57. Monopoli, M. P.; Aberg, C.; Salvati, A.; Dawson, K. A., Biomolecular coronas provide the biological identity of nanosized materials. *Nat Nanotechnol* **2012,** *7* (12), 779-786.

58. Bantz, C.; Koshkina, O.; Lang, T.; Galla, H.-J.; Kirkpatrick, C. J.; Stauber, R. H.; Maskos, M., The surface properties of nanoparticles determine the agglomeration state and the size of the particles under physiological conditions. *Beilstein Journal of Nanotechnology* **2014,** *5*, 1774-1786.

59. Matsumoto, H.; Koyama, Y.; Tanioka, A., Interaction of proteins with weak amphoteric charged membrane surfaces: effect of pH. *Journal of Colloid and Interface Science* **2003,** *264* (1), 82-88.

60. Patil, S.; Sandberg, A.; Heckert, E.; Self, W.; Seal, S., Protein adsorption and cellular uptake of cerium oxide nanoparticles as a function of zeta potential. *Biomaterials* **2007,** *28* (31), 4600-7.

61. Meder, F.; Kaur, S.; Treccani, L.; Rezwan, K., Controlling mixed-protein adsorption layers on colloidal alumina particles by tailoring carboxyl and hydroxyl surface group densities. *Langmuir* **2013,** *29* (40), 12502-12510.

62. Price, W. S.; Tsuchiya, F.; Arata, Y., Lysozyme Aggregation and Solution Properties Studied Using PGSE NMR Diffusion Measurements. *Journal of the American Chemical Society* **1999,** *121* (49), 11503-11512.

63. Farka, Z.; Kovar, D.; Skladal, P., Rapid detection of microorganisms based on active and passive modes of QCM. *Sensors (Basel)* **2014,** *15* (1), 79-92.

64. Chen, L.; Zhang, J., Bioconjugated magnetic nanoparticles for rapid capture of gram-positive bacteria. **2012**.

65. Jin, Y.; Deng, J.; Liang, J.; Shan, C.; Tong, M., Efficient bacteria capture and inactivation by cetyltrimethylammonium bromide modified magnetic nanoparticles. *Colloids Surf B Biointerfaces* **2015,** *136*, 659-65.

For table of contents only: